Review │ Received 5 March 2026; Revised 30 April 2026; Accepted 14 May 2026; Published 5 June 2026
https://doi.org/10.55092/ ae20260003

Photopolymerisation-extrusion coupled moulding: a new paradigm and trend outlook for 3D printing of ceramic precursors

Linzhe Zhang[1], Zhen Wang[1,2,*], Chuanzhen Huang[1,2], Longhua Xu[1], Shuiquan Huang[1], Meina Qu[1], Zhengkai Xu[1], Dijia Zhang[1], Baosu Guo[1], Tianye Jin[1] and Xiaodan Wang[1]

[1] School of Mechanical Engineering, Yanshan University, Qinhuangdao, China
[2] State Key Laboratory of Crane Technology, Yanshan University, Qinhuangdao, China

* Correspondence author; E-mail: wangzhen@ysu.edu.cn.

Highlights:

- Proposes photopolymerisation-extrusion coupled moulding for ceramic precursor 3D printing.
- Reviews binary/ternary/multicomponent polymer-derived ceramic precursor systems. Clarifies photopolymerization reaction and volumetric shrinkage mechanisms of PDCs.
- Analyzes non-Newtonian extrusion flow rheology of ceramic precursor slurries.
- Outlines bottlenecks and future routes for high-performance PDC additive manufacturing.

Abstract: Ceramic materials are indispensable in aerospace, energy, and biomedical fields due to their high hardness, heat resistance, and corrosion resistance. However, their inherent brittleness makes it difficult to fabricate complex structures via traditional forming methods. 3D printing provides an effective near-net-shape route, among which Polymer-Derived Ceramics (PDCs) have become a research hotspot owing to binder-free composition, molecular design flexibility, and low-temperature sinterability. This review focuses on photopolymerisation-extrusion coupled moulding as a core strategy to resolve the long-standing trade-off between high precision and low defects in PDC 3D printing. We systematically review the material systems of ceramic precursors, analyze the principles of photopolymerisation-based printing for PDCs, clarify the reaction mechanisms, volumetric shrinkage mechanisms, and extrusion flow behaviors of photopolymerisation-assisted extrusion 3D printing. Emphasis is placed on how coupling mitigates contradictions between precision and defects, improves interlayer bonding, and reduces warpage and cracking. Finally, we summarize key bottlenecks and propose targeted future development directions, providing a clear reference for advancing high-performance ceramic precursor additive manufacturing.

Keywords: photopolymerisation-extrusion coupling moulding; ceramic precursors; additive manufacturing; polymer-to-ceramic conversion; volumetric shrinkage; precision-defect trade-off

1. Introduction

With technological advancement, demands for material performance continue to rise across aerospace, biomedicine, and other fields. Ceramic materials, owing to their high hardness, heat resistance, wear resistance, and corrosion resistance, have become pivotal materials in these sectors [1]. However, the inherent high hardness and brittleness of ceramics render their manufacturing and processing challenging. Traditional forming methods such as dry pressing and slip casting can only produce components with simple structures, severely limiting the application scope of ceramic materials [2].

Ceramic 3D printing technology has advanced rapidly since its initial application in the 1990s. Based on forming principles, it encompasses various techniques including Stereolithography (SLA) [3], Digital Light Processing (DLP) [4], and Fused Deposition Modelling (FDM) [5]. Each technology possesses distinct advantages in print dimensions, speed, and precision, rendering them suitable for different scenarios. For instance, SLA and DLP are well-suited for ceramic slurries and resin solutions, offering high resolution and surface quality; FDM is cost-effective but exhibits lower precision and mechanical properties; Selective Laser Sintering (SLS) [6] requires no support structures but involves expensive equipment and significant powder wastage. Specific characteristics are summarised in Table 1.

Table 1. Characteristics of common additive manufacturing technologies.

Forming Principle	Technology	Accuracy	Speed	Surface Quality
Extrusion Moulding	FDM	100 μm–100 mm [7]	20–150 mm/s [8]	Xydirection ±0.1 mm–±0.3 mm Zdirection ±0.05 mm [18]
Extrusion Moulding	DIW	200 μm–100 mm [9]	15–50 mm/s [10]	Ra values as low as 6.8μm
Photopoly merisation	SLA	100 μm–300 mm [11]	20–500 mm/h [12]	Xydirection ±0.04 mm–±0.1 mm Zdirection ±0.04 mm–±0.1 mm [19]
Photopoly merisation	DLP	100 μm–100 mm [13]	100–1000 mm/h [14]	Xydirection ±0.06 mm–±0.1 mm zdirection ±0.06 mm–±0.1 mm
Powder Binding Moulding	IJP	200 μm–10 mm [15]	5–20 mm/s	Varies by equipment and materials
Powder Binding Moulding	SLS	200 μm–500 mm [16]	2.2 L/h [17]	± 0.3 mm

The advent of 3D printing (additive manufacturing) technology has opened new avenues for near-net-shape fabrication of complex three-dimensional ceramic components. Currently, 3D printing of ceramic materials primarily employs stereolithography techniques [20], in which ceramic powder is mixed with organic binders to form a slurry. This slurry is then cured layer by layer to create a green body, which undergoes debinding and high-temperature sintering to produce the final component [21]. However, the use of binders in this technique poses challenges in producing fully dense, crack-free ceramic components with high geometric fidelity. In contrast, binderless 3D-printed polymer-to-ceramic conversion significantly mitigates these issues. It enables enhanced density through multiple impregnation and pyrolysis cycles, while its molecular design flexibility and low-temperature ceramicisation characteristics have made it a research hotspot in ceramic additive manufacturing [22].

Precursor conversion ceramics technology has been applied across multiple domains, including ceramic matrix composites, fibres, and functional ceramics, driving advancements in aerospace, energy,

electronics, and biomedical industries [23]. As illustrated in Figure 1, within aerospace, it enables the fabrication of high-temperature-resistant components such as engine combustion chambers [24]; in energy, it is suitable for fuel cell materials [25]; in electronics, it can be employed for electrocatalytic energy conversion reactions [26]; and in biomedicine, precursor ceramics hold potential as catalytic carriers or bio-scaffolding materials [27].

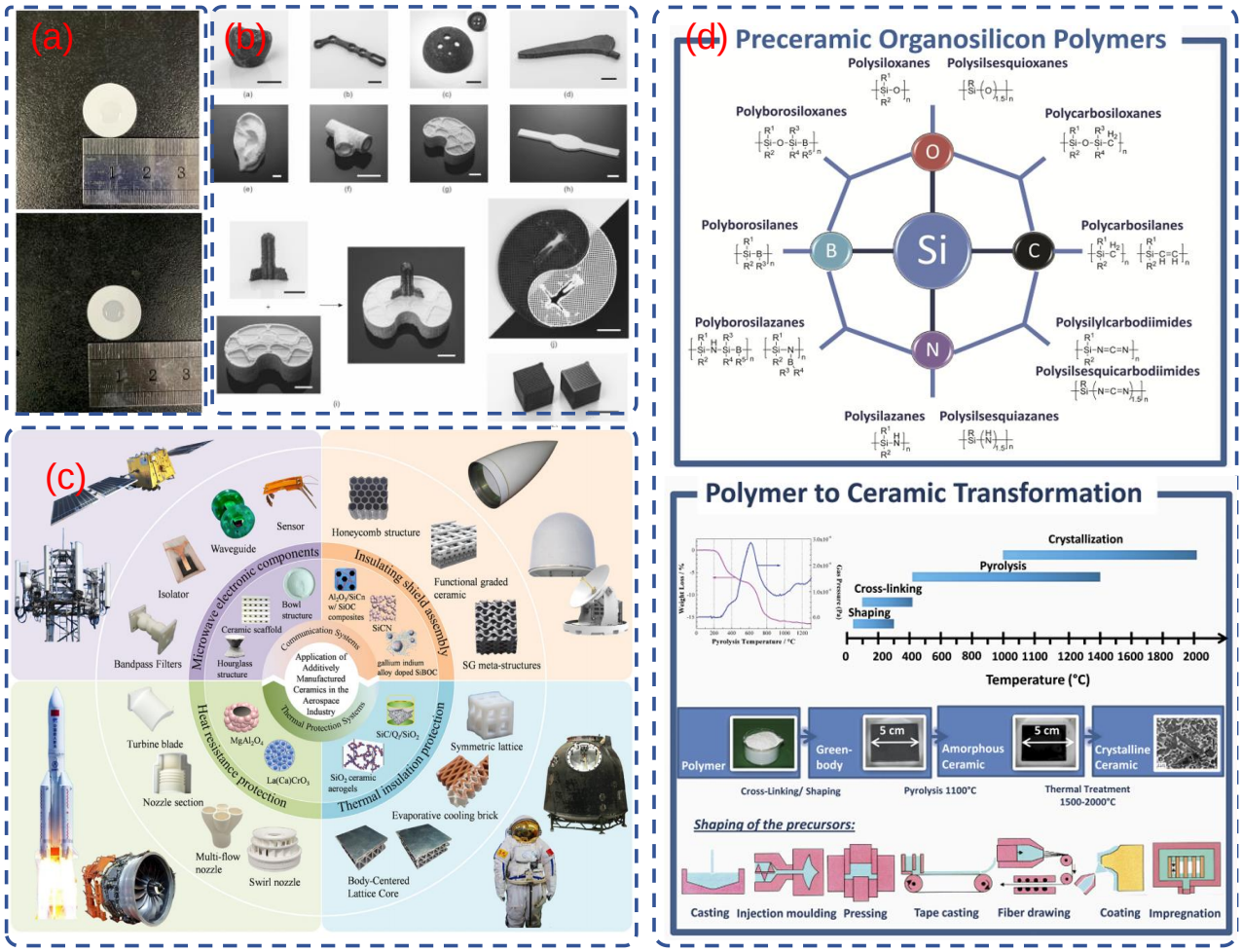

Figure 1. Typical application examples of ceramics in various fields.**(a)** Applications of precursor ceramics in the electronics sector [28]; **(b)** Applications of precursor ceramics in the biomedical sector [29]; **(c)** Applications of precursor ceramics in the aerospace sector [30]; **(d)** Applications of precursor ceramics in the energy sector [31].

2. Current research status of ceramic precursor material systems

Ceramic precursors refer to a class of polymers synthesised chemically that can be converted into ceramic materials through heat treatment. Polymer-derived ceramics (PDCs) are produced by subjecting ceramic precursors to cross-linking and curing to form thermosetting polymers, followed by high-temperature pyrolysis to yield ceramic products [32]. Compared to traditional powder-based ceramic preparation, ceramic precursors offer molecular design flexibility, allowing performance modification of PDCs through the introduction of additional functional groups. Depending on precursor type, sintering temperature, and atmosphere, PDCs can be fabricated in various systems, including

binary, ternary, and quaternary compositions. Capable of sintering at relatively low temperatures (1000–1300 ℃) while exhibiting temperature resistance exceeding 1500 ℃, PDCs possess functional characteristics such as electrical conductivity and luminescence alongside excellent biocompatibility, demonstrating significant advantages in porous ceramic fabrication [33].

2.1. Conversion of binary system polymer precursors into ceramics

Binary precursor systems (mainly SiC, Si_3N_4, ZrB_2) serve as the foundational material platform for PDCs, with SiC being the most extensively studied. These systems were first developed to achieve basic ceramic conversion and establish fundamental processing-structure-property relationships, laying the groundwork for subsequent ternary and multicomponent systems. In 1976, Yajima *et al.* pioneered the synthesis of polycarbosilane (PCS) and prepared SiC fibers via melt spinning and pyrolysis, marking the birth of precursor-derived ceramics [34].

PCS precursors vary in side-chain groups and molecular weight, including poly(methylsilane) derivatives, as illustrated in Figure 2a. Blending polysiloxanes with differing chemical structures can also yield SiC precursor solutions. Researchers [35] prepared SiC by pyrolysing commercial polysiloxanes under vacuum at temperatures ranging from 250 to 1600 ℃. The PCS pyrolysis process comprises cross-linking, polymer degradation, ceramicisation, and crystallisation stages: cross-linking occurs at room temperature to 300 ℃, forming a solid; degradation and conversion to ceramic occur at 300–800 ℃, releasing small molecules and forming new chemical bonds; Amorphous SiC nucleates at 800–1000 ℃; above 1000 ℃, the amorphous state transforms into β-SiC nanocrystals, with pronounced crystallisation at 1200 ℃. Partial conversion of β-SiC to α-SiC occurs above 1400 ℃.

To address pyrolysis-induced volume shrinkage and low ceramic yield, researchers have employed fillers such as metal ions and metal powders. Huang *et al.* [36] from the Chinese Academy of Sciences incorporated Si nanopowder into the precursor, increasing ceramic yield from 72% to 81.8% while reducing free carbon content. Yao *et al.* [37] from Xiamen University added SiC(rGO)p powder, achieving a 3D-SiC(rGO)px ceramic yield of 94.5% with pyrolysis shrinkage reduced to 5%. Wang *et al.* [38] from the National University of Defense Technology achieved a HfC-SiC ceramic yield of 77.8 wt% by mixing hafnium polyoxide with polydimethylsiloxane, followed by pyrolysis at 1600 ℃.

2.2. Ternary system precursor-converted ceramics

To overcome the insufficient thermal stability and functional limitations of binary systems in extreme environments, ternary systems were developed by introducing a third element. This expansion significantly improves high-temperature stability, oxidation resistance, and electromagnetic performance, addressing the performance bottlenecks of binary PDCs. Among them, SiOC and SiCN are the most representative.

As shown in Figure 2b, the ternary system primarily comprises SiCN, SiOC, SiBN, SiBC, and others. PDC-SiOC is synthesised via curing pyrolysis using polysiloxane (PSO) as a precursor, wherein Si atoms are simultaneously bonded to C and O atoms. Its unique structure confers exceptional thermal stability and oxidation resistance; reducing free carbon content further enhances oxidation resistance [39]. At approximately 1300 ℃, SiOC ceramics undergo carbon thermal reduction decomposition. During

pyrolysis, amorphous phases undergo phase separation, precipitating SiC crystals; higher temperatures yield increased SiC crystal formation.

PDC-SiCN utilises polynitrosilane (PSZ/PSN) as its precursor. At pyrolysis temperatures below 1500 ℃, it predominantly exists in an amorphous state. Upon further heating, Si_3N_4 and SiC nanocrystals form, whilst the free carbon graphitises [40]. PDC-SiBN utilises polyborosilazane (PBSZ) as its precursor, with the precursor type influencing its structure and properties. The team led by Liu Shidong at Northwestern Polytechnical University obtained PDC-SiBN ceramics by pyrolysing different precursors at 900–1500 ℃ under an NH_3 atmosphere. They discovered that pyrolysis formed Si-N-O structures, with precursor composition influencing the ceramic's thermal stability and electromagnetic wave transmission properties [41].

Additionally, researchers have investigated PDC-BCN ceramics. Bill *et al.* at the Max Planck Institute for Metals prepared BCN ceramics using diazobicyclohexane and ammonium borane complexes as monomeric precursors [42]; Zhang *et al.* from Harbin Institute of Technology synthesised precursor polymers using boron chloride, hexanediamine, and aniline as monomers, yielding low-density hydrophobic h-BCN after pyrolysis, which can serve as an electromagnetic wave absorber [43].

2.3. Quaternary and multicomponent systems: precursor conversion ceramics

To further push the high-temperature limit beyond 2000 ℃and achieve multifunctional integration, quaternary and multicomponent systems were designed by introducing B, N, or other elements. These systems represent the highest level of molecular design in current PDCs, solving the stability failure of ternary systems under ultra-high temperatures and enabling applications in harsh aerospace conditions.

Pyrolysis of mixed carbide or nitride precursors yields polycrystalline dichalcogenides (PDCs) such as SiBCN and SiOCB. In the 1990s, the Riedel *et al.* at Darmstadt University of Technology, Germany, synthesised SiBCN using PBSZ as a precursor, discovering that adding boron elevated the decomposition temperature to over 2000 ℃ [44]. The Jia *et al.* at Harbin Institute of Technology prepared SiBCN using liquid PBSZ, curing at 150 ℃, followed by pyrolysis at 1000–1700 ℃. The ceramic yield reached 54%, exhibiting an amorphous structure below 1400 ℃, with β-SiC and BN(C) crystallisation occurring above 1500 ℃ [45].

The phase composition of SiBCN ceramics varies with process conditions, with reported precursors including boron-doped polysilazanes. Huang Qing's team employed polyboron-containing polysilazane as a crosslinking agent, reacting it with polysilazane to yield crosslinked polyborosilazane (CPBCS). Curing and pyrolysis of this compound produced SiBCN ceramics. These maintained an amorphous state between 800–1400 ℃, with boron suppressing carbon thermal reduction reactions. and forms a protective layer on the surface during high-temperature heating in air, exhibiting temperature resistance up to 1600 ℃.

To enhance the temperature resistance of SiOC, researchers extensively investigated boron doping. Bai Hongwei from Harbin Institute of Technology incorporated boric acid into the precursor polymethylhydroxysiloxane (PMHS), yielding amorphous SiOCB ceramics via pyrolysis at 1000 ℃ with a yield of 80%–86%. Boron *et al.* increased crosslinking density, and with rising temperature, phase separation occurred, resulting in graphite microcrystals [46].

SiOCN ceramics exhibit superior high-temperature stability compared to SiOC. The nitrogen element elevates the carbon thermal reduction reaction temperature. These ceramics can be synthesised

via oxidative pyrolysis of polysilazane or pyrolysis of SiOC precursors under an NH_3 atmosphere [47]. Bai *et al.* obtained SiOCN ceramics by mixing tetramethylcyclotetrasiloxane with allylamine, crosslinking and curing the mixture, followed by high-temperature pyrolysis. Pyrolysis at 1000 °C yielded an amorphous state, with structural and phase changes occurring at elevated temperatures [48,49].

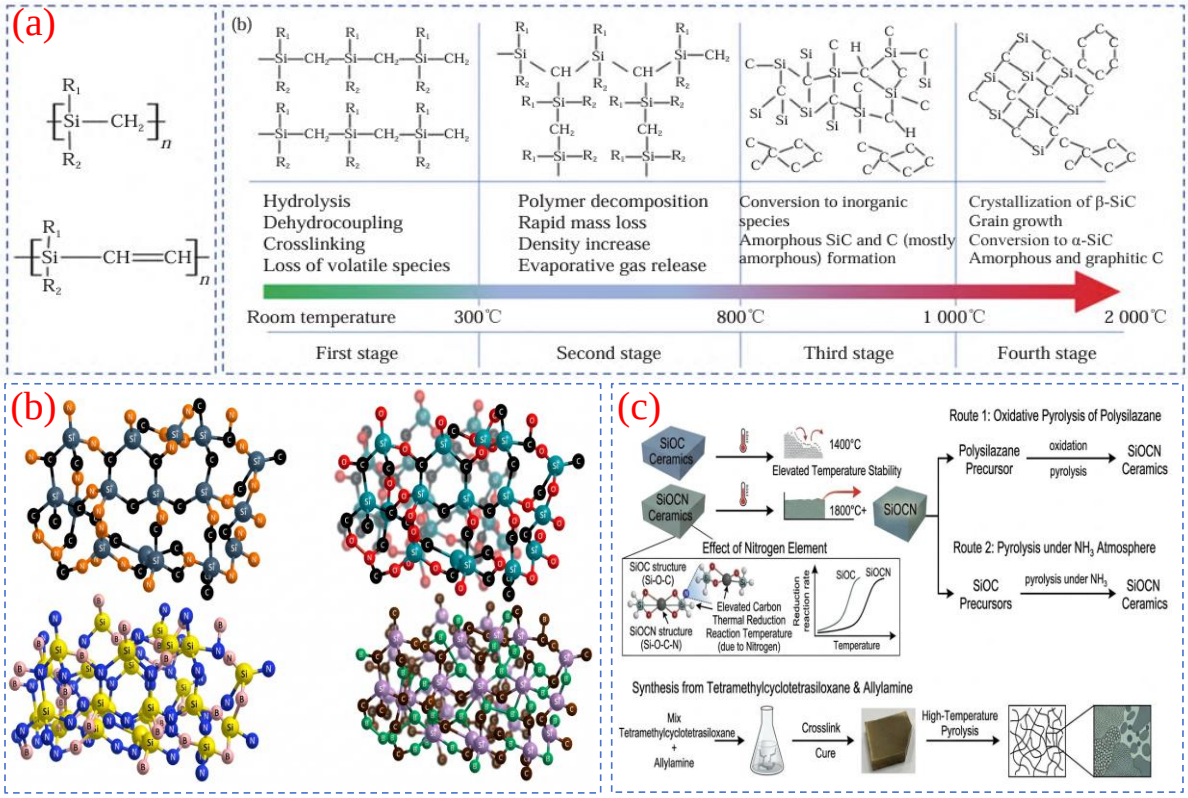

Figure 2. Classification of polymer precursor-converted ceramic material systems. **(a)** Chemical structural units of the binary system precursor ceramic polysilane (PCS) and the pyrolysis process of PCS precursors converting to SiC [50]; **(b)** Crystal structures of several typical ternary ceramics; **(c)** Synthetic route of SiOCN ceramics from tetramethylcyclotetrasiloxane and allylamine.

3. Photopolymerization-based additive manufacturing of polymer-derived ceramics

Photopolymerization-based additive manufacturing has become the most promising 3D printing technique for polymer-derived ceramics owing to its high precision [51,52], superior surface quality, and fast fabrication rate. Unlike conventional ceramic slurry photopolymerization, ceramic precursors can be rationally designed at the molecular level to introduce photopolymerizable groups without relying on excessive organic binders. This strategy fundamentally eliminates defects caused by debinding and enables the fabrication of near-net-shape ceramics with low defects [53]. Based on different photosensitization strategies, the research can be classified into three categories: photocurable functional group modification, two-component photopolymerizable oligomer blending, and multifunctional acrylate composite systems, which together form the core material system for photopolymerization 3D printing of ceramic precursors.

To clarify the characteristics and applicable scenarios of different strategies, a concise comparison is listed in Table 2.

Table 2. Comparison of photopolymerization strategies for polymer-derived ceramic 3D printing.

Strategy	Typical System	Ceramic	Key Strengths	Key Limitations
Grafted photocurable [54–58]	PVZ-IEM MK-TMSPM acrylated polysilazane	SiOC SiCN SiBCN	High precision low defect uniform shrinkage	Complex synthesis
Two-component blended precursors [59,60]	Thiol-siloxane vinyl-siloxane	SiOC	Simple, fast curing O_2-insensitive	Low ceramic yield
Multifunctional acrylate composites [61,62]	Precursor polyfunctional acrylate	SiC SiOC	High green strength, good printability	High shrinkage

3.1. Photocurable functional group-modified ceramic precursors

Covalently grafting photocurable groups such as acrylates, methacrylates, and vinyl groups onto the backbones of polysiloxanes, polysilazanes, and polycarbosilanes is the most effective approach to achieve high-precision photopolymerization printing with a single component. This strategy allows the regulation of curing behavior, crosslinking density, and ceramic yield at the molecular level, and has become the mainstream design for SiOC, SiCN, and SiBCN systems.

As illustrated in Figure 3a, Pham *et al.* [54] modified vinyl polysilazane with isocyanatoethyl methacrylate at a ratio of 1:4. Using two-photon absorption crosslinking and subsequent pyrolysis at 600 °C, SiCN ceramics with complex microstructures were fabricated, and nano-silica was found to effectively reduce dimensional deformation. As illustrated in Figure 3b, Li *et al.* [55] grafted 1,1-bis isocyanateonto polyvinylpolysilazane to introduce photopolymerizable groups, realizing two-photon stereolithography of SiCN-based ceramics with outstanding microstructural fidelity. As depicted in Figure 3c, Zanchetta *et al.* [56] developed an MK-TMSPM slurry using methylsilsesquioxane and 3-propyl trimethoxysilane. After SLA printing and pyrolysis at 1000 °C, SiOC ceramics with a density of approximately 2.2 g/cm³ and smooth surfaces were obtained, representing a classic system for photopolymerizable SiOC.

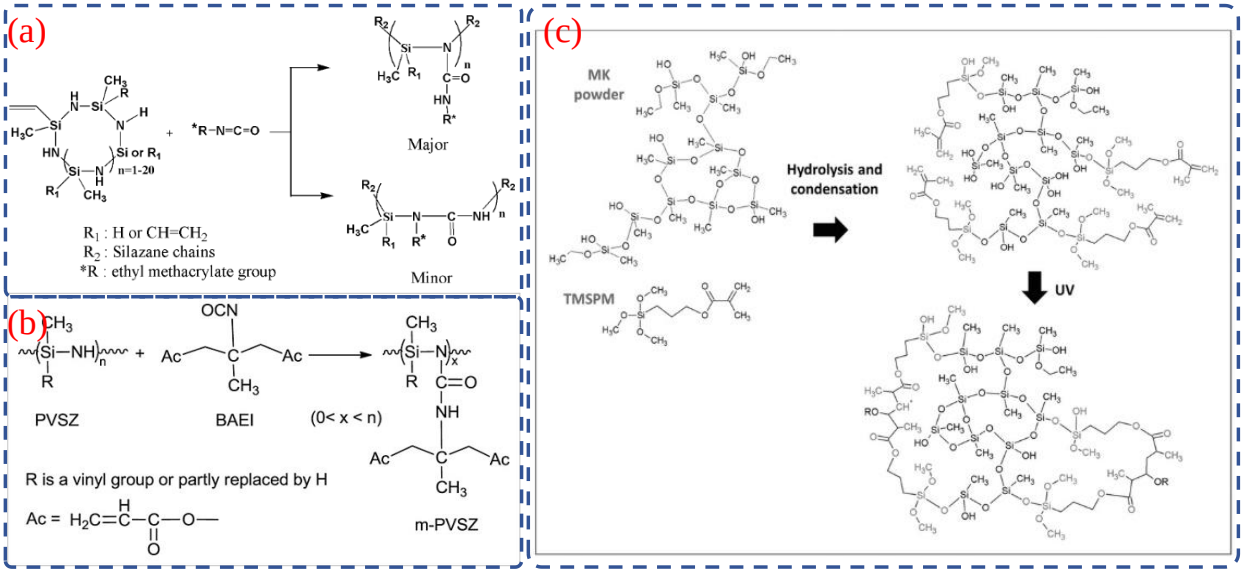

Figure 3. Photocurable functional group-modified ceramic precursors. **(a)** Precursor ceramics modified by scholar Pham [54]; **(b)** SiCN ceramics incorporating photopolymerisation groups [55]; **(c)** Slurry for preparing MK-TMSPM by Zanchetta [56].

In the field of photopolymerization of silicon-based non-oxide ceramics, Salameh's group established a systematic method for precursor photosensitization. By blending methylsilsesquioxane with 1,6-hexanediol diacrylate, crack-free SiOC ceramic monoliths were successfully fabricated via UV-LCD 3D printing and pyrolysis at 1000 °C [57]. Further boron modification and acrylate grafting enabled the direct UV photolithography of SiBCN precursors for the first time, producing crack-free microstructures ranging from 20 to 200 μm with surface roughness below 3 nm and Young's modulus of 60 GPa, which can be directly applied in MEMS and microfluidic devices [58]. This molecular-level modification overcomes the bottleneck that traditional polysilazanes and polysiloxanes cannot be directly photopolymerized. Moreover, higher crosslinking density leads to more uniform pyrolysis shrinkage and fewer defects.

3.2. Two-component photopolymerizable oligomer-blended ceramic precursors

Physical blending of two complementary photopolymerizable oligomers provides a rapid route to photosensitive systems without complex covalent synthesis, combining the advantages of simple processing and tunable performance.

Eckel *et al.* [59] blended mercaptopropyl methylsiloxane and vinylmethoxysiloxane with UV-radical photoinitiators to formulate a resin suitable for desktop SLA printers. After pyrolysis at 1000 °C in argon, high-density SiOC ceramics were obtained, providing a universal solution for consumer-grade photopolymerization equipment. Hundley *et al.* [60] systematically studied the dimensional evolution from printing to pyrolysis using the same two-component system, reporting a linear shrinkage of 29.7 ± 1.2% and volumetric shrinkage of 64.9 ± 1.6%, with uniform isotropic shrinkage, supporting accurate dimensional compensation.

This system shows unique advantages in thiol-ene photopolymerization: vinyl and thiol groups are insensitive to oxygen inhibition, enabling fast curing and uniform crosslinking. The surface roughness of printed SiOC (Ra ≈ 18 μm) is significantly lower than that of acrylate blending systems (Ra ≈ 50 μm) [57]. Meanwhile, two-component blending allows flexible adjustment of ceramic compositions; for example, the introduction of boron or aluminum-containing oligomers enables the direct preparation of multicomponent ceramics such as SiBCN and SiAlCN for high-temperature and corrosion-resistant applications.

3.3. Multifunctional acrylate-blended ceramic precursors

Blending ceramic precursors with multifunctional acrylate monomers improves forming efficiency and green body strength through the rapid curing of acrylates. This balanced approach achieves good printability and reliable ceramic yield, and is widely used in the preparation of high-strength SiC and SiOC components.

As illustrated in Figure 4a, de Hazan *et al.* blended allylhydridopolycarbosilane with 1,4-butanediol diacrylate, investigated the photopolymerization mechanism, and printed intricate high-precision 3D structures via SLA [61]. After pyrolytic sintering at 1300°C in argon, SiC-rich ceramics with enhanced flexural strength were obtained. As depicted in Figure 4b, Fu *et al.* dissolved methylsilsesquioxane and 3-methacryloxypropyltrimethoxysilane in solvent, hydrolyzed them under acidic conditions, introduced metal alkoxides and trimethylolpropane triacrylate to prepare a slurry. After DLP printing of octahedral truss

structures and pyrolysis at 1200 ℃, high-hardness and high-compressive-strength SiOC ceramics were achieved, realizing integrated structural and functional design [62].

For monolithic catalytic applications, the combination of 3D-printed SiOC and atomic layer deposition represents a breakthrough. Salameh *et al.* [63] used UV-LCD 3D-printed SiOC ceramic monoliths as supports and precisely loaded palladium nanoparticles via ALD. When applied in aqueous Suzuki-Miyaura coupling reactions, the catalyst achieved a yield of up to 82%, with Pd leaching below 25 ppb and high activity retention after 8 cycles. The 3D grid structure significantly improved mass transfer efficiency compared with powder catalysts. This system integrates multifunctional acrylate curing, polymer-to-ceramic conversion, and vapor-phase functionalization, representing the advanced trend from structural ceramics to functional ceramics.

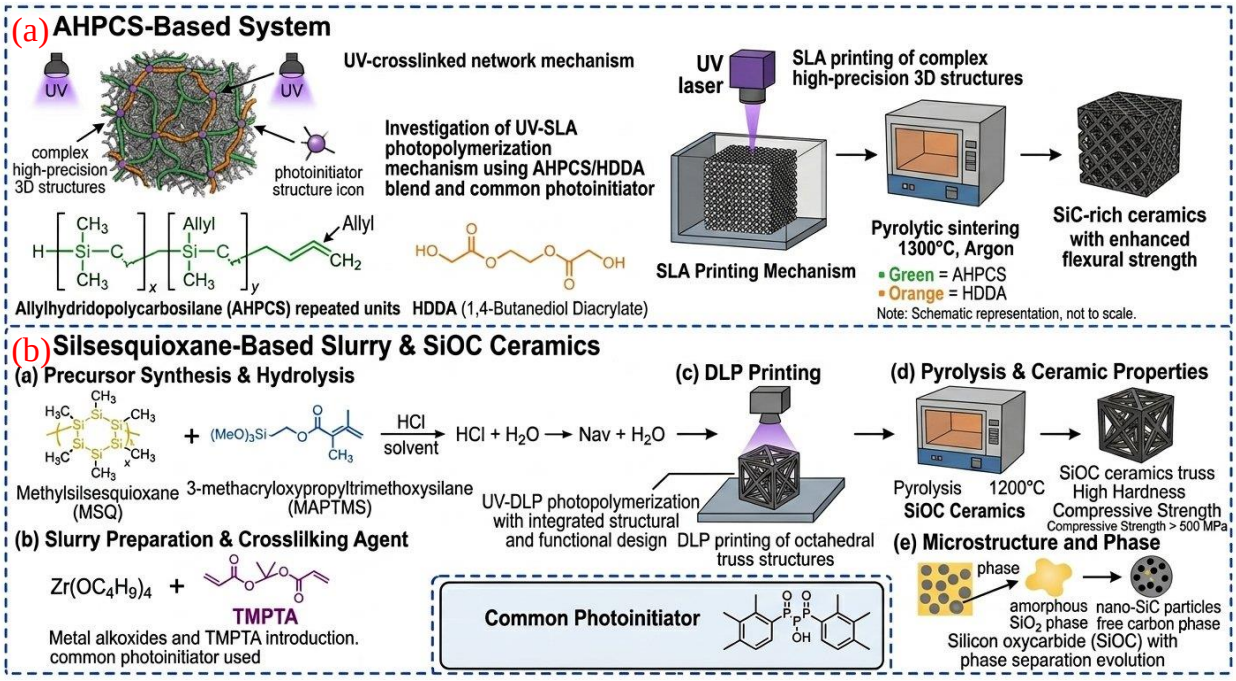

Figure 4. Schematic diagram of photocuring forming mechanism for precursor blended acrylate system. **(a)** Schematic diagram of the photopolymerisation mechanism of AHPCS/bis-acrylate systems; **(b)** Schematic illustration of the photopolymerizable slurry components and reaction mechanisms for digital light processing 3D printing of polymer-derived Si-based ceramics.

4. Photopolymerisation extrusion coupling moulding technology

4.1. Technical principles and equipment composition

Photopolymerisation-extrusion coupled moulding is a synchronous hybrid forming technology that simultaneously implements extrusion deposition and *in-situ* UV curing, which is the essential difference from traditional DIW featuring extrusion first followed by post-curing and SLA/DLP adopting layered surface curing. The material is extruded from the nozzle in a continuous filament; immediately upon extrusion, it is irradiated by a coaxial/paraxial UV light source to complete rapid photocuring, thus freezing the filament shape instantly, suppressing sagging and deformation, and realizing layer-by-layer stable stacking. This synchronous coupling fundamentally solves the contradiction between extrusion

fluidity and dimensional stability, achieving high material adaptability empowered by extrusion characteristics as well as high precision brought by photopolymerisation performance.

The coupled equipment is specially designed for synchronous extrusion-curing: Mechanical system: Equipped with a precision piston/screw extrusion module and a conical nozzle with polished inner wall to reduce wall slip and ensure stable filament output; Light source system: Adopts a coaxial/paraxial UV-LED laser assembly matching the precursor absorption peak, with real-time adjustable light intensity to match extrusion speed; Control system: Real-time linkage of extrusion flow rate, platform moving speed, and UV illumination intensity to ensure coupling synchronization; Auxiliary system: Includes constant temperature feeding and online monitoring to stabilize slurry viscosity and curing uniformity [64].

This synergistic coupling strategy delivers prominent advantages over conventional single-mode printing technologies by addressing their intrinsic bottlenecks. In comparison to direct ink writing, *in-situ* photopolymerization effectively inhibits filament sagging and interlayer deformation, which substantially improves dimensional precision and the fabrication feasibility of overhanging structures. Different from stereolithography and digital light processing, this hybrid strategy removes the strict requirement for low-viscosity and high-flowability slurries, enabling excellent processability for high-viscosity precursors with high ceramic yields. Meanwhile, it alleviates oxygen inhibition and enhances interlayer bonding strength. Collectively, such an integrated manufacturing route minimizes the dependence on auxiliary supports, simplifies the fabrication procedure, and restrains crack generation caused by heterogeneous stress accumulation.

4.2. Photopolymerisation moulding and reaction mechanism

Photopolymerisation 3D printing employs a radiation source to irradiate liquid photopolymer resin, triggering a chain chemical reaction that links numerous small-molecule monomers or prepolymers together to form a highly cross-linked polymer [65]. Figure 5a illustrates the photopolymerisation reaction mechanism.

Photocuring systems primarily comprise oligomers, photoinitiators, and monomers (reactive diluents) [66]. Among these, low molecular weight polymers containing unsaturated functional groups-oligomers-constitute the highest proportion of the system, determining the fundamental properties of the cured product. Reactive diluents regulate system viscosity, thereby influencing curing rate and material performance. Photoinitiators generate radicals or ions capable of initiating polymerisation upon light exposure, being pivotal to the initiation of the curing reaction. Figure 5b illustrates the classification of stereolithography processes.

Photopolymerisation is primarily categorised by mechanism into radical, cationic, and anionic photopolymerisation, with the former two being more widely applied.

Radical photopolymerisation: The most extensively applied system in light curing, primarily utilising (meth)acrylate and unsaturated polyester monomers. Photoinitiators generate radicals upon light exposure, which react with monomer carbon-carbon double bonds to initiate chain growth. Characterised by a short induction period and rapid polymerisation rate, the reaction ceases immediately upon light removal [67].

Cationic photopolymerisation: A significant component of photopolymerisation technology, utilising monomers such as epoxides, vinyl ethers, and propylene ethers. Active fragments include

protonic acids (primary role) and radicals. Compared to radical photopolymerisation, it exhibits a longer induction period and slower polymerisation rate, with reactions continuing after light exposure ceases [68].

Anionic photopolymerisation: Less commonly applied, this process utilises photo-alkylating agents as initiators, with amine fragments as the primary reactive species. Compared to cationic photopolymerisation, this system effectively avoids the substrate corrosion associated with photo-acidifying agent systems [69].

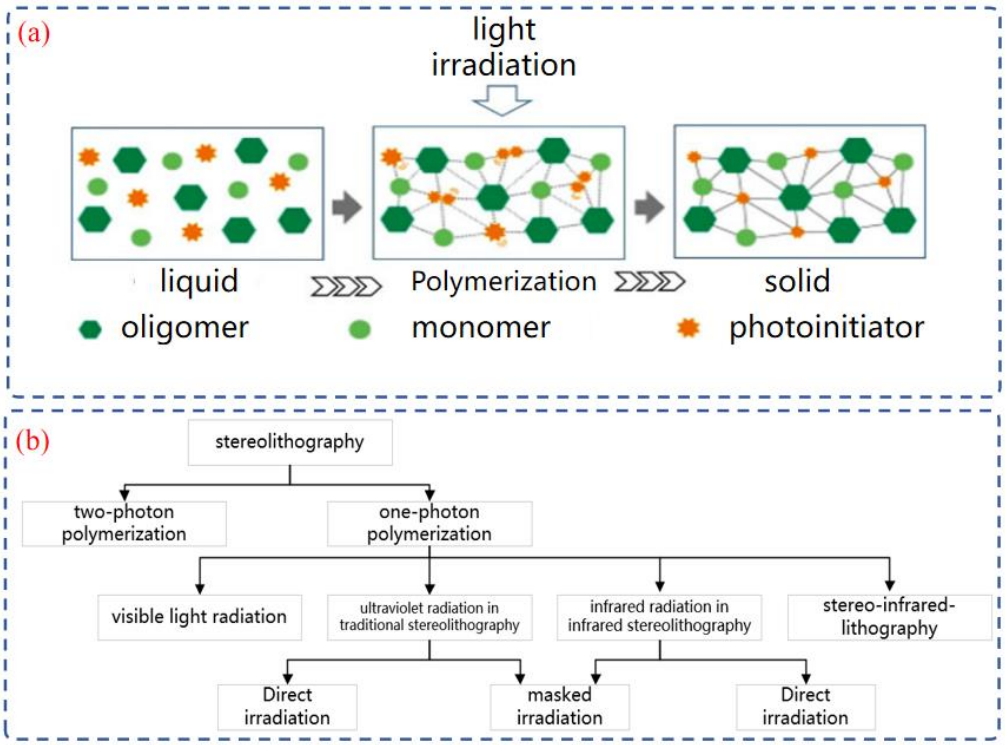

Figure 5. Reaction mechanism of photopolymerization and classification of photocuring forming processes. **(a)** Mechanism of photopolymerisation reactions; **(b)** Several photopolymerisation modes in stereolithography processes.

4.3. Photopolymerization volume shrinkage and strategies for shrinkage reduction

4.3.1. Photopolymer volume shrinkage

Photopolymerization volume shrinkage is a critical issue affecting the dimensional accuracy and structural stability of ceramic components in UV-curing-assisted extrusion 3D printing. This phenomenon is closely related to molecular interaction mechanisms and reaction kinetics, and it causes a series of adverse effects that restrict the high-quality forming of ceramic precursor 3D printing. As illustrated in Figure 6, at the molecular level, in conventional polymerization reactions, monomer molecules are initially held together by van der Waals forces, with an intermolecular distance of approximately 0.3–0.5 nm. After polymerization, covalent bonds are formed between molecules, and the bond length is reduced to 0.154 nm [70]. This sharp decrease in intermolecular spacing inevitably leads to volume contraction of the system. For photopolymerization reactions, in addition to this common factor, there is a unique stress accumulation effect. The reaction rate of radical photopolymerization systems is extremely fast, usually completing within tens of seconds, which is much shorter than the relaxation time required for polymer chain motion.

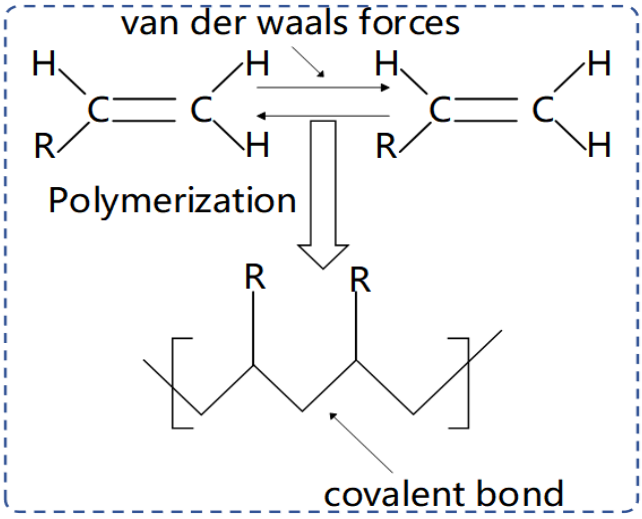

Figure 6. Variation in intermolecular distances during radical photopolymerization.

As a result, polymer chains are solidified and locked before fully extending to a thermodynamic equilibrium state, remaining in the system in a coiled conformation, which further aggravates the degree of volume shrinkage. Ceramic precursors with different chemical compositions exhibit distinct shrinkage characteristics due to differences in molecular structure, crosslinking density, and pyrolysis behavior, as summarized in the following Table 3.

Table 3. Volume shrinkage comparison for different ceramic precursor systems.

Ceramic System	Precursor Type	Linear Shrinkage	Volumetric Shrinkage	Ceramic Yield
SiC	Polycarbosilane	25%–32% [34]	60%–70% [35]	72%–82% [36]
SiOC	Polysiloxane	28%–32% [56]	64%–68% [56]	75%–86% [57]
SiCN	Polysilazane	30%–35% [54]	66%–72% [54]	65%–75% [55]
SiBCN	Boron-doped polysilazane	22%–28% [58]	55%–62% [58]	54%–70% [59]

Volume shrinkage exerts significant negative impacts on the quality of printed parts. First, unreleased internal stress raises the surface tension of the cured layer and weakens interlayer adhesion. In rigid substrates or components, this easily induces voids or even fractures; in flexible structures, it may cause warping deformation and damage the overall geometric integrity of the part [71,72]. Second, volume shrinkage directly leads to deviations between the actual dimensions of printed parts and the design values, reducing geometric precision [73]. In fields requiring strict dimensional accuracy, such as precision ceramic components for aerospace, microelectronic packaging ceramics, and biomedical ceramic scaffolds, such precision deviations severely limit the application of the technology and make it difficult to meet high-fidelity forming requirements. Therefore, solving the problem of photopolymerization volume shrinkage is a key step to improve the quality of ceramic precursor photopolymerization-extrusion coupling molding.

4.3.2. Strategies for reducing photopolymerization shrinkage

In photopolymerisation reactions, volume shrinkage is a prevalent issue that significantly constrains the quality and application scope of photopolymerised products. To overcome this challenge, researchers

have developed a series of effective methods to reduce volume shrinkage by addressing multiple aspects, including raw materials, volume shrinkage compensation, and additives.

(1) Selection of low-shrinkage monomers and oligomers

In terms of raw material selection, the use of low-shrinkage monomers and oligomers is a direct and effective strategy. The shrinkage degree of photopolymerizable materials is directly related to the functional group density in the structure of monomers and oligomers. Higher functional group density leads to greater reaction crosslinking and more significant curing shrinkage [74]. Increasing the proportion of high-molecular-weight reactive monomers in the matrix resin can reduce the photopolymerization conversion rate and final volume shrinkage [75]. Modifying epoxy acrylate with polyurethane side chains can increase the molecular weight and cohesive energy of the resin, reduce functional group density, and significantly lower the shrinkage rate [76]. Developing new monomers with large molecular weight, high rigidity, and low functional group density can also reduce the loss of molecular spacing during curing from the source and achieve shrinkage reduction [77].

(2) Shrinkage compensation using cyclic monomers

The introduction of cyclic monomers is a common method to compensate for shrinkage. Cyclic monomers undergo ring-opening reactions during cationic polymerization, and their volume expansion effect can partially offset polymerization shrinkage. After ring-opening polymerization of typical epoxy monomers, the shrinkage rate of epoxy resin is only 2%–6% [78], much lower than that of conventional radical polymerization systems. Ring-opening polymerization of polycyclic monomers can even achieve volume expansion [79]. Expandable monomers such as spiroepoxy carboxylates and spiroepoxy carbonates used to modify epoxy resins can effectively alleviate or even offset polymerization shrinkage, and controlled addition can achieve near-zero shrinkage or slight expansion [80].

(3) Modification via functional additives

Adding specific additives can also effectively improve volume shrinkage. Adding an appropriate amount of thiol-ene hybrid resin to acrylate photopolymerization systems can reduce curing shrinkage while ensuring high reactive group conversion. Thiol chain transfer agents delay the gelation process, shifting most shrinkage to before gelation, relieving internal stress and maintaining mechanical properties [81]. Adding fillers to photopolymer resins can simultaneously improve the mechanical properties after curing, reduce curing shrinkage, and lower the thermal expansion coefficient. Fillers reduce the functional group density of the system and remain stable in volume during curing, thus offsetting part of the shrinkage [82]. Spherical nanoparticles are more effective than irregular particles in reducing shrinkage. Silane-modified reactive nano-SiO_2 can form physical entanglement and chemical crosslinking with the matrix resin, efficiently reducing shrinkage and polymerization stress, improving particle-resin compatibility, reducing agglomeration, and ensuring full curing of the composite [83]. It should be noted that the filler content must be moderate; excessive content will increase system viscosity, complicate processing, hinder stress release, and affect printing and forming effects.

5. Analysis of the extrusion flow process

5.1. Analysis of the extrusion process

The extrusion flow behavior of ceramic precursor slurry directly determines filament diameter uniformity, shape stability, and printing quality. Since most precursors are non-Newtonian fluids,

establishing a rheological model is essential to predict flow state, optimize nozzle structure, and match extrusion pressure and speed. This section introduces classical constitutive equations and Reynolds number criteria, and combines practical cases to illustrate their guiding role in process optimization. Printing materials for ceramic precursors are typically non-Newtonian fluids, characterised notably by a non-linear relationship between shear stress and shear rate [84].

$$\tau = k \cdot \gamma^n = k\left(-\frac{du}{dr}\right)^n \tag{1}$$

This equation is used to identify the shear-thinning behavior of ceramic precursor inks and provides a basis for adjusting slurry viscosity suitable for stable extrusion. In the equation: τ denotes the shear stress applied to the fluid; k represents the coefficient characterising the fluid's consistency index, where a higher value indicates greater viscosity; h denotes the shear rate; n is the power-law exponent measuring the degree of non-Newtonian behaviour, with n=1 corresponding to Newtonian fluids, $n < 1$ to pseudoplastic fluids, and $n > 1$ to thixotropic fluids. Wu *et al.* [64] formulated a zirconia ceramic slurry with a volume fraction of 45%, exhibiting a density of approximately 2285 kg/m ³ As depicted in Figure 7a, the slurry demonstrates typical non-Newtonian behaviour [85]. Ding Zhicheng *et al.* formulated silicone ink. To characterise the material properties of the ink, the Herschel-Bulkely model was employed to describe a typical non-Newtonian fluid. Taking logarithms of both sides of the Herschel-Bulkely model yielded the formula, from which it can be seen that exhibits a linear relationship with; combining experimentally measured ink shear stress-shear rate data (Figure 7b), the equation was fitted to determine material constitutive parameters. The fitting yielded an $R^2 > 0.95$, confirming the shear-thinning behaviour of this silicone ink. The Herschel-Bulkley model is adopted to characterize the yield stress and rheological response of pastes, enabling accurate description of flow behavior during extrusion.

$$\tau=\tau_0+K\gamma^n \tag{2}$$

$$\log_{10}(\tau-\tau_0)=\log_{10}K+n\log_{10}\gamma \tag{3}$$

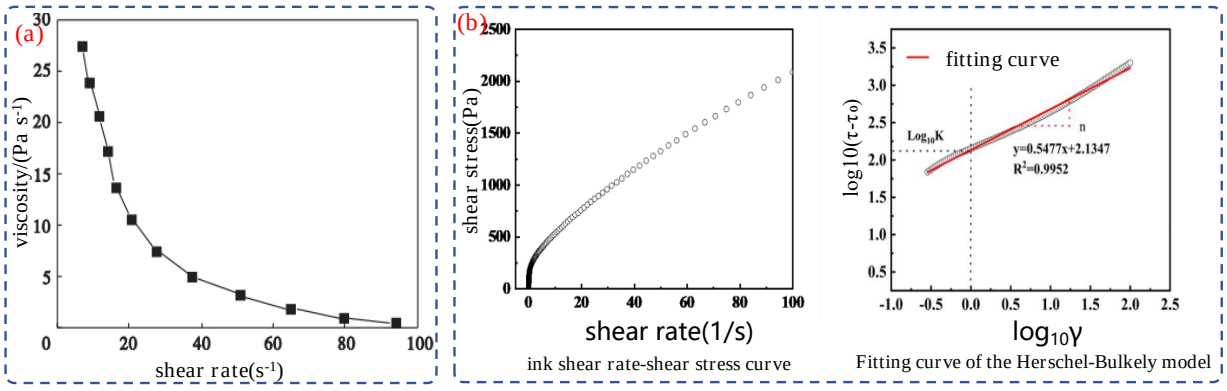

Figure 7. Viscosity versus shear rate relationship of ceramic precursor slurry. **(a)** Shear stress-shear rate curve of ceramic precursor ink; **(b)** Fitting curve of the Herschel-Bulkely rheological model.

The flow behaviour of ceramic precursor slurry within 3D printing extrusion systems directly determines filament quality and printing stability [86]. Its flow process requires a comprehensive analysis integrating channel geometry, fluid properties, and boundary conditions. The flow path in a

typical extrusion system comprises the barrel storage section, screw conveying section, and conical nozzle section. Conical nozzles are predominantly employed in extruders [87] as they effectively reduce flow resistance, substantially decreasing the driving force required to extrude the slurry.

When viscous fluids move within flow channels, molecular cohesive forces and momentum exchange generate viscous shear stresses between adjacent fluid layers, impeding relative motion [88]. Overcoming this resistance and conducting losses along the pipeline requires external driving forces provided by screws or pistons, a process accompanied by irreversible dissipation of mechanical energy. For non-Newtonian fluids such as ceramic precursor slurries, their flow state can be determined by the Reynolds number for power-law fluids. Typically, when $Re < 2000$, laminar flow occurs, with velocity distributed parabolically within the flow channel (maximum velocity at the centre of the pipe, minimum at the wall). whereas when $Re > 4000$, the flow transitions to turbulence, with a flatter velocity distribution. However, turbulence readily causes agglomeration of the slurry or entrainment of air bubbles; hence, actual printing operations are predominantly controlled within the laminar flow regime. The flow regime of a fluid is determined by its Reynolds number, with the Reynolds number Re [89] for non-Newtonian fluids satisfying:

$$Re = \frac{D_0^n V^{2-n} \rho}{8^{n-1} K \left(\frac{3n+1}{4n} \right)^n} \tag{4}$$

Reynolds number calculation is used to ensure laminar flow regime and avoid turbulence-induced bubbles, agglomeration, and discontinuous filament extrusion. Where: ρ is the fluid density; D_0 is the flow channel diameter; K is the viscosity coefficient. The flow rate of a power-law fluid in laminar flow within a circular channel satisfies [90]:

$$Q = \int_0^R u 2\pi r dr = \frac{\pi n R^3}{3n+1} \left(\frac{\Delta p R}{2LK} \right)^{\frac{1}{n}} \tag{5}$$

Flow rate modeling helps quantitatively match extrusion pressure and nozzle output to achieve uniform filament diameter. In the equation: p denotes the pressure drop within the flow channel; R represents the channel radius; L signifies the channel length. The flow rate Q within the channel characterises its functional relationship with the pressure drop Δp within the channel. Through this relationship, the variation in extrusion velocity during the printing process can be further calculated to determine compliance with extrusion moulding requirements. The average flow velocity at the cross-section during the flow process is

$$\overline{V} = \frac{Q}{\pi R^2} = \frac{nR}{3n+1} \left(\frac{\Delta p R}{2LK} \right)^{\frac{1}{n}} \tag{6}$$

Average velocity calculation is used to coordinate extrusion speed and platform scanning speed, ensuring dimensional accuracy and layer uniformity. Near the wall surface, fluids form a boundary layer with extremely low velocity due to adsorption forces and van der Waals forces, resulting in a slow sliding motion along the wall known as wall slip [91]. Should the wall slip effect become pronounced, it may cause the actual flow rate to deviate from theoretical calculations and even trigger extrusion instability. In engineering calculations, the influence of wall slip is typically mitigated by modifying boundary conditions or optimising flow channel surface roughness.

5.2. Mechanisms governing photopolymerisation of materials

Photopolymerisation extrusion moulding requires synergistic optimisation of the 'slurry-light source-process' triad, with the core objective being rapid curing and setting of the slurry post-extrusion while ensuring interlayer bonding strength and geometric precision. Specific control pathways encompass both slurry formulation optimisation and light source parameter adjustment.

5.2.1. Slurry-based control

The particle size, volume fraction, and dispersion of ceramic particles within the slurry significantly influence light transmission efficiency and curing effectiveness. Griffith *et al.* [92] proposed that the penetration depth of light within the slurry [93] and the presence of substances therein exhibit the following relationship:

$$D_{\mathrm{p}} \propto \frac{2d_{50}}{3}\frac{\lambda}{\phi\, s}\frac{n_0^2}{\Delta n^2} \tag{7}$$

In the equation, d_{50}, λ, ϕ, s, n_0, and Δn denote the mean particle diameter, wavelength, particle volume fraction, interparticle spacing, solvent refractive index, and refractive index difference between ceramic particles and solvent respectively.

Considering the viscosity of ceramic photopolymerisation slurries [94], the overall viscosity increases at the macroscopic level with rising solid content. At a ceramic powder volume fraction Φ, this viscosity increase can be evaluated using the Krieger-Dougherty equation [95]:

$$\eta_r = \frac{\eta}{\eta_0} = \left(1 - \frac{\beta \cdot \Phi}{\phi_0}\right)^{-[\eta]\phi_0} \tag{8}$$

In the equation, η_r represents the relative viscosity of the resin, η denotes the suspension viscosity at extremely low shear rates, η_0 is the viscosity of the organic medium, ϕ_0 represents the volume fraction of the filler when the particles are densely packed, and $[\eta]$ is the intrinsic viscosity of the particles. Reducing the viscosity of high-solids-content ceramic slurries is crucial for ensuring the smooth progression of the curing reaction during the forming process.

5.2.2. Light source parameter regulation

The light source wavelength must match the absorption spectrum of the photosensitiser in the paste. For instance, when employing α-hydroxyketone photosensitisers such as Irgacure 819, a UV-LED light source with a wavelength of 365-405 nm should be selected [96]. At this wavelength, the photosensitiser's molar extinction coefficient ε exceeds 10^4 L/(mol·cm), enabling efficient radical generation to initiate polymerisation. Photocuring control must balance curing speed and shrinkage stress. Increasing light intensity from 10 mW/cm² to 50 mW/cm² reduces curing time from 30 seconds to 5 seconds, but increases volumetric shrinkage from 5% to 8%, potentially inducing internal stresses. In practical applications, a 'gradient light intensity' strategy is employed: during initial extrusion, low light intensity (10–20 mW/cm²) initiates slow polymerisation to minimise shrinkage stress; subsequently, high light intensity (30–50 mW/cm²) accelerates curing to enhance production efficiency [97].

Curing is only achieved when the exposure energy E (E = light intensity × exposure time) reaches the critical exposure threshold. According to Jacobs' equation [98].

$$D_C = D_p \cdot ln\left(\frac{E_0}{E_c}\right) \quad (9)$$

Here, denotes the cured thickness, represents the penetration depth of light in the ceramic suspension, indicates the exposure energy, and signifies the critical exposure dose. When $Ec < 2$, $DC <$ Dp, resulting in insufficient curing; when $Ec > 5$, DC approaches saturation, readily causing over-curing and edge blurring. Typically, Ec is controlled at 3-4 to align the cured thickness with the layer thickness, thereby ensuring interlayer adhesion.

Furthermore, environmental control during printing must not be overlooked [99]. For instance, elevated temperatures (e.g, from 25 ℃ to 40 ℃) accelerate photopolymerisation rates, reducing curing time by 20%–30%. However, humidity must be maintained below 50% to prevent moisture reacting with siloxane groups in the slurry to form hydroxyl groups, which impairs ceramicisation efficiency. In practical printing, adjustments should be made based on process parameters and environmental conditions to meet the requirements for precision ceramic components.

6. Summary and outlook

6.1. Summary

Photopolymerisation-extrusion coupled moulding has emerged as a transformative paradigm for ceramic precursor additive manufacturing, addressing the longstanding dilemma in polymer-derived ceramic (PDC) fabrication: the trade-off between high forming precision and shrinkage-induced defects. This review summarizes material advances, photopolymerisation mechanisms, shrinkage control strategies, and extrusion rheological behaviors, following a progressive logic from binary to ternary and multicomponent precursor systems. Binary SiC-based precursors laid the material foundation but suffered from excessive shrinkage and limited thermal stability; ternary SiOC, SiCN, and SiBN systems improved oxidation resistance and structural stability; multicomponent SiBCN and SiOCB ceramics further enhanced ultra-high-temperature tolerance and functional diversity.

The coupling technology overcomes the weaknesses of single-mode printing, enabling *in-situ* solidification, enhanced interlayer adhesion, and reduced support dependence. Rheological modelling provides quantitative guidance for flow stability and parameter optimization, facilitating reliable near-net-shaping of complex ceramic components for aerospace, energy, electronics, and biomedicine applications.

6.2. Outlook

Despite substantial progress, critical challenges centered on the precision-defect trade-off restrict industrial translation. Future research shall focus on breakthroughs in core directions to elevate the technology's maturity. Precursor molecular engineering for low-shrinkage high-performance systems requires rational design of flexible chain architectures, regulated functional group density, and expandable ring-opening moieties, intrinsically mitigating volumetric shrinkage while boosting ceramic yield and thermomechanical properties. Multiphysics coupled modelling and simulation demands the

establishment of integrated frameworks encompassing fluid flow, light propagation, reaction kinetics, and heat diffusion, enabling accurate prediction of curing uniformity, residual stress, and dimensional deviation to replace empirical parameter tuning. *In-situ* intelligent closed-loop control calls for the integration of high-speed imaging, temperature/stress sensing, and machine learning algorithms, realizing dynamic modulation of extrusion states, light intensity, and environmental conditions for consistent high-quality forming. Scalable industrial-grade manufacturing systems necessitate the development of large-format, high-throughput equipment with adaptive curing atmospheres and integrated post-processing modules, meeting industrial demands for stability, repeatability, and cost efficiency. As summarized in Figure 8, these key bottlenecks and corresponding optimization strategies for advancing photopolymerisation-extrusion coupled moulding toward practical industrial applications. Advancing material design, process intelligence, and equipment engineering will propel ceramic additive manufacturing toward higher precision, reliability, and broader industrial deployment.

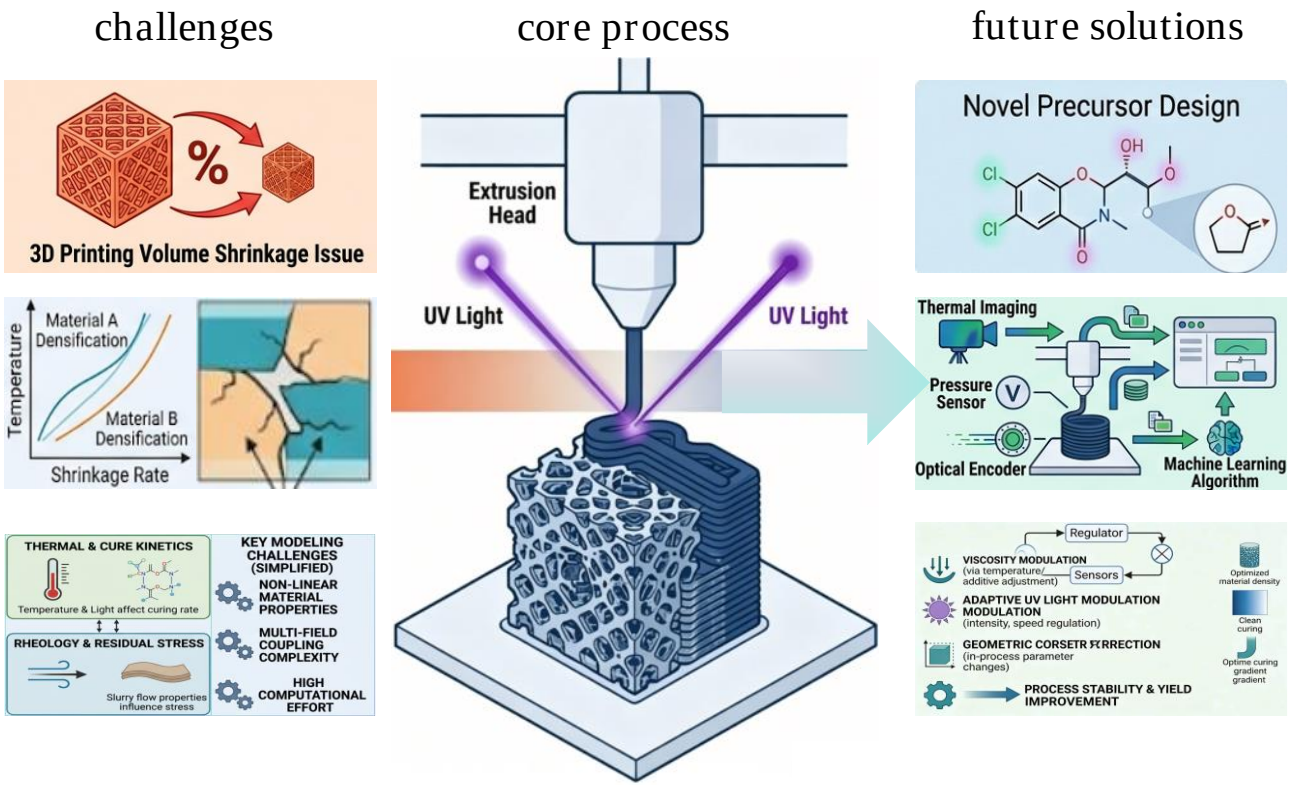

Figure 8. Schematic diagram of current technical bottlenecks and corresponding breakthrough strategies for photopolymerisation-extrusion coupled moulding of ceramic precursors.

Data availability statement

No new data were generated or analyzed in this review study. All content and analyses are based on previously published literature and existing public research findings.

Declaration of generative AI and AI-assisted technologies

The authors declare that generative AI tools (DeepSeek and ChatGPT) were only utilized for language editing, grammatical polishing and expression optimization in this manuscript. No AI tools were

involved in research design, theoretical analysis, content creation or conclusion derivation. All scientific content, viewpoints and results are independently completed by the authors, who take full responsibility for the originality, integrity and accuracy of the manuscript.

Acknowledgments

This work is supported by National Natural Science Foundation of China (52305513, 52575542, 52305425), and Science Research Project of Hebei Education Department (BJK2024053).

Authors' contribution

Linzhe Zhang: conceptualization, methodology, investigation, writing—original draft; Zhen Wang: supervision, project administration, writing—review and editing; Chuanzhen Huang: funding acquisition, resources, academic supervision; Longhua Xu: formal analysis, rheological data analysis; Shuiquan Huang: literature collection, data curation; Meina Qu: investigation, mechanism sorting and validation; Zhengkai Xu: visualization, literature collation; Dijia Zhang: literature review, process mechanism analysis; Baosu Guo: parameter validation, theoretical analysis; Tianye Jin: figure organization, writing—review and editing; Xiaodan Wang: manuscript polishing, content revision. All authors reviewed and approved the final version of the manuscript.

Conflicts of interest

Chuanzhen Huang holds the position of Advisory Board Member for *Advanced Equipment* and has not peer reviewed or made any editorial decisions for this paper.

References

[1] Wu S, Zhao Y, Li W, Liu W, Wu Y, *et al.* Research progresses on ceramic materials of thermal barrier coatings on gas turbine. *Coatings* 2021,11(1):79.

[2] Li B, Wang S, Chen J, Li Z, Shan W, *et al.* 3D Printing of LuAG: Ce transparent ceramics for laser-driven lighting. *Ceram. Int.* 2023, 49(23PB):38708–38716.

[3] Zandinejad A, Das O, Barmak A, Kuttolamadom M, Revilla-León M. The flexural strength and flexural modulus of stereolithography additively manufactured zirconia with different porosities. *J. Prosthodont.* 2021, 31(5):434–440.

[4] Seo H, Kim H, Choi H, Kim D, Galbadrakh A, *et al.* Ceramic bodies without warping using epoxide-acrylate hybrid ceramic slurry for photopolymerization-based 3D printing. *Int J Appl Ceram Technol.* 2023, 21(1):76–88.

[5] Ziadia A, Habibi M, Kelouwani S. Digital twin-driven real-time optimization of layer-specific surface roughness in FDM 3D printing. *Prog. Addit. Manuf.* 2025, 10(11):10053–10076.

[6] Mazhar H, Osswald T, Negrut D. On the use of computational multi-body dynamics analysis in SLS-based 3D printing. *Addit. Manuf.* 2016, 12:291–295.

[7] Xie W, Li N, Jiang J, Lu J, Cai H, *et al.* DLP photocuring 3D printing and GO/transition metal composite electrodes: Synergistic design for sustainable energy catalytic oxygen evolution electrodes. *Int. J. Hydrogen Energy.* 2025, 176:151457.

[8] Palaniappan A, Krishnan R, Uthappan K, Ramesh T. Analysis on mechanical properties and characterization of polylactic acid/wood infill composites manufactured by fused deposition modeling. *J. Mater. Eng. Perform.* 2025, 35(6):5161–5175.

[9] Zhao C, Wang T, Zhou J, Liu D, Hu Y, *et al.* Pulsed-switchable strategy and relative-pressure control optimizing multi-ceramics 3D printing integrated with laser-assisted curing. *Addit. Manuf.* 2025, 11:104946.

[10] Wang Y, Ding Y, Yu K, Dong G. Advancing high-performance composites in additive manufacturing through pre-impregnation and direct ink writing for scalable 3d printing. *J. Compos. Sci.* 2025, 9(5):218.

[11] Garc á-Gil I, Rodr guez Alonso V, Tobar Arribas C, Mosaddad S, Pel áez J, *et al.* Dental casts for fixed dental prostheses printed with sla technology: influence of external shell thickness and printing orientation. *Materials* 2025, 18(10):2246.

[12] Ramos-Oca ña S, Cabrera-Moreta V. Validation of velocity in microchannels with a retention system due to unevenness manufactured by 3D printing (SLA). In *Proceedings of the Defect and Diffusion Forum*, Online, April, 2025, pp. 243–260.

[13] Zhao W, Singh P, Han J, Shen, F, Hu K, *et al.* Precision-optimized process control in DLP printing of ultra-thin zirconia prostheses: a multi-factor accuracy analysis. *Dent. Mater*. 2025.

[14] Wu D, Zhao Z, Zhang Q, Qi H, Fang D. Mechanics of shape distortion of DLP 3D printed structures during UV post-curing. *Soft Matter* 2019, 15(30):6151–6159.

[15] Elkaseer A, Schneider S, Deng Y, Scholz S. Effect of process parameters on the performance of drop-on-demand 3d inkjet printing: geometrical-based modeling and experimental validation. *Polymers* 2022, 14(13):2557.

[16] Baloni S, Sharma S, Singh J, Negi S. SLS process parameter optimization to improve surface quality and accuracy of polyamide parts. *Int. J. Manuf. Mater. Mech. Eng.* 2021, 11(4):57–74.

[17] Kim GD, Oh YT. A benchmark study on rapid prototyping processes and machines: quantitative comparisons of mechanical properties, accuracy, roughness, speed, and material cost. *Proc. Inst. Mech. Eng., Part B: J. Eng. Manuf.* 2008, 222(2):201–215.

[18] Madheswaran S, Venkatesh Raja K, Venkatachalam R. Assessment of material extrusion process parameters on the surface quality enhancement of 3D printed PLA specimens. *Int. J. Mater. Res.* 2025, 116(8):676–693.

[19] Abbasi M, V áz P, Silva J, Martins P. Head-to-head evaluation of FDM and SLA in additive manufacturing: performance, cost, and environmental perspectives. *Appl. Sci.-Basel*. 2025, 15(4):2245–2245.

[20] Fern ández-Abia AI, Mart ínez-Sanchez Á, Pel áez-Pel áez S, Rodr guez-Gonz ález P, Castro-Sastre MÁ. Microstructural transformation and defect analysis in alumina ceramics components manufactured by stereolithography additive manufacturing technology. *Int. J. Adv. Manuf. Technol.* 2025, pp. 1–9.

[21] Sun J, Li H, Mu Y, Mu B, Chen Y, *et al.* Improving wear resistance of 3D printed alumina-based ceramics via sintering temperature. *China Foundry* 2025, 22(2):151–162.

[22] Xing R, Xu G, Qu N, Zhou R, Yang J, *et al.* 3D printing of liquid-metal-in-ceramic metamaterials for high-efficient microwave absorption. *Adv. Funct. Mater.* 2023, 34(31):2307499.

[23] Fu S, Zhu M, Zhu Y. Organosilicon polymer-derived ceramics: an overview. *J. Adv. Ceram.* 2019, 8(4):457–478.

[24] Huang W, Wang Y, Ning Z, Mao S, Xue Z, *et al.* Design of lightweight and antioxidant SiCnws/SiC(Mox, rGO) nanocomposite from molybdenum-modified precursors for aerospace vehicle components. *Ceram. Int.* 2023, 49(15):25998–26014.
[25] Wen Q, Qu F, Yu Z, Graczyk-Zajac M, Xiong X, *et al.* Si-based polymer-derived ceramics for energy conversion and storage. *J. Adv. Ceram.* 2022, 11(2):197–246.
[26] Guo Y, Sugahara Y. Polymer-derived ceramics for electrocatalytic energy conversion reactions. *Int. J. Appl. Ceram. Technol.* 2022, 20(1):8–23.
[27] Murugavel R. Ceramic and porous framework metal silicates and phosphates from molecular precursors: an ever-evolving ambient synthesis approach. *Emergent Mater.* 2019, 2(3):273–294.
[28] Lin Z. Preparation of SiC by conversion of polymer modified with nanocarbon materials and its radiation resistance. Master's Thesis, Zhengzhou University, 2022.
[29] Liu G, He Y, Liu P, Chen Z, Chen X, *et al.* Development of bioimplants with 2D, 3D, and 4D additive manufacturing materials. *Engineering*, 2020, 6(11):63–88.
[30] Colombo P, Mera G, Riedel R, Soraru GD. Polymer-derived ceramics: 40 years of research and innovation in advanced ceramics. *J. Am. Ceram. Soc.* 2010, 93(7):1805–1837.
[31] Scheffler M. Processing of ceramics from polysil(sesquioxane)-type precursors: coatings, tapes, tailored surfaces, and porosity control. *Adv. Eng. Mater.* 2023, 25(17):2300290.
[32] Xiong S. Conversion of photocurable 3D-printed polymer precursors to SiOC ceramics. Master's Thesis, Shenzhen University, 2023.
[33] Chen M. Research progress on 3D printing technology of polymer-derived ceramics. *J. Ceram.* 2020, 41(2):150–156.
[34] Yajima S, Hayashi J, Omori M, Okamura K. Development of a silicon carbide fibre with high tensile strength. *Nature* 1976, 261(5562):683–685.
[35] Hackbarth H, Key T, Ackley B, Opletal G, Rawal A, *et al.* Uncovering atomic-scale polymer-to-ceramic transformations in SiC polymer derived ceramics from polycarbosilanes. *J. Eur. Ceram. Soc.* 2024, 44(4):1932–1945.
[36] Wang Y, Ma L, Pei X, Zhuo W, Huang J, *et al.* Residual carbon trapping effect of nano Si for stoichiometric SiC derived from polycarbosilane and its application in SiCf/SiC composites with largely improved thermal conductivity. *J. Eur. Ceram. Soc.* 2024, 44(13):7482–7489.
[37] Zhuang K, Lin S, Huang W, Liao L, Zheng Y, *et al.* Realizing high ceramic yield and low shrinkage of *in-situ* formed lightweight 3D-SiC(rGO)px polymer-derived ceramics with excellent fracture toughness. *Ceram. Int.* 2020, 46(17):27426–27436.
[38] Wang X, Zhang L, Wang Y. Preparation of HfC-SiC ultra-high-temperature ceramics by the copolycondensation of HfC and SiC precursors. *J. Mater. Sci.* 2022, 57(7):4467–4480.
[39] Wang Y, Zujovic Z, Wu J, Wang H, Gao W. Robust and ultrafine silicon oxycarbide fiber mats prepared by a spinning-aid free electrospinning/sol-gel method. *Mater. Lett.* 2021, 283:128696.
[40] Li Q. Electromagnetic absorbing properties and its optimization of PDCs-SiC(N) ceramics and composites. Doctoral Thesis, Northwestern Polytechnical University, 2015.
[41] Zhan Y, Li W, Jiang T, Fasel C, Ricohermoso III E, *et al*. Boron-modified perhydropolysilazane towards facile synthesis of amorphous SiBN ceramic with excellent thermal stability. *J. Adv. Ceram.* 2022, 11(7):1104–1116.

[42] Bill J, Riedel R, Passing G. Amin-borane als precurs oren für borcarbidnitrid. *Z. Anorg. Allg. Chem.* 1992, 610(4):83–90.
[43] Zhang T, Zhang J, Wen G, Zhong B, Xia L, *et al.* Ultra-light h-BCN architectures derived from new organic monomers with tunable electromagnetic wave absorption. *Carbon* 2018, 136:345–358.
[44] Riedel R, Kienzle A, Dressler W, Ruwisch L, Bill J, *et al.* A silicoboron carbonitride ceramic stable to 2000 °C. *Nature* 1996, 382(6594):796–798.
[45] Niu Z, Li D, Jia D, Yang Z, Lin K, *et al.* Comparative study on the micro structure evolution and crystallization behavior of precursor-derived and mechanical alloying derived SiBCN. *J. Eur. Ceram. Soc.* 2024, 44(2):668–678.
[46] Zhang X, Liu C, Hong C, Han J, Han W, *et al.* Sol-gel-derived SiBOC ceramics with highly graphitized free carbon. *Ceram. Int.* 2015,41(10):15292–15296.
[47] Shao G, Ding C, Yu G, Xu R, Huang X. Bridged polysilsesquioxane-derived SiOCN ceramic aerogels for microwave absorption. *J. Am. Ceram. Soc.* 2022, 106(4):2407–2419.
[48] Wang B, Song Y, Zhang X, Chen K, Liu M, *et al*. Polymer derived SiBCN(O) ceramics with tunable element content. *Ceram. Int.* 2022, 48(7):10280–10287.
[49] Bai H. Preparation and properties of B or N modified SiOC base ceramic. Doctoral Thesis, Harbin Institute of Technology, 2011.
[50] Zhou Y, Lu K. Polymer-derived high-temperature nonoxide materials: a review. *Adv. Eng. Mater.* 2023, 25(9):2200967.
[51] Bishop V, Mathur CS, Nguyen N, Sharma B, Drouin M, *et al*. A review of direct ink writing of polymer derived ceramics. *Virtual Phys. Prototyp.* 2025, 20(1):2499938.
[52] Chaudhary R, Degbedzui JS, Biesuz M, Sorarù GD. Structural and microstructural evolution of fused filament fabricated SiOC(N) via polymer-derived ceramics route. *Open Ceram.* 2025, 22:100839
[53] Compton BG, Bui PP, Romberg SK, Kemp JW, Reed JL, *et al.* 3D-printed SiC-microfiber-reinforced polymer-derived ceramic with high strength at elevated temperature. *J. Am. Ceram. Soc.* 2025, 108(12):e70143.
[54] Pham T, Kim D, Lim T, Park S, Yang D, *et al.* Three-dimensional SiCN ceramic microstructures via nano-stereolithography of inorganic polymer photoresists. *Adv. Funct. Mater.* 2006, 16(9):1235–1241.
[55] Li Y, Ahn K, Kim D. Synthesis and properties of UV curable polyvinylsilazane as a precursor for micro-structuring. *Polym. Adv. Technol.* 2015, 26(3):245–249.
[56] Zanchetta E, Cattaldo M, Franchin G, Schwentenwein M, Homa J, *et al.* Stereolithography of SiOC ceramic microcomponents. *Adv. Mater.* 2016, 28(2):370–376.
[57] Hippolyte D, Philippe M, Chrystelle S. UV-curable inorganic precursors enable direct 3D printing of SiOC ceramics. *Int. J. Appl. Ceram. Technol.* 2022, 20(1):141–152.
[58] Hanniet Q, Petit E, Calas-Etienne S, Etienne P, Aissou K, *et al.* Rational design of SiBCN microstructures using direct photolithography of patternable preceramic photoresists. *Mater. Des.* 2022, 223:111234
[59] Eckel Z, Zhou C, Martin J, Jacobsen A, Carter W, *et al.* Additive manufacturing of polymer-derived ceramics. *Science* 2016, 351(6268):58–62.

[60] Hundley J, Eckel Z, Schueller E, Cante K, Biesboer S, *et al.* Geometric characterization of additively manufactured polymer derived ceramics. *Addit. Manuf.* 2017, 18:95–102.
[61] de Hazan Y, Penner D. SiC and SiOC ceramic articles produced by stereolithography of acrylate modified polycarbosilane systems. *J. Eur. Ceram. Soc.* 2017, 37(16):5205–5212.
[62] Fu Y, Xu G, Chen Z, Wang D, Lao C, *et al.* Multiple metals doped polymer-derived SiOC ceramics for 3D printing. *Ceram. Int.* 2018, 44(10):11030–11038.
[63] Dory H, Petit E, El-Sayegh S, Badouric L, Castro V, *et al.* Monolith catalyst design by combining 3d printing and atomic layer deposition: toward green palladium-catalyzed cross-coupling reactions. *Adv. Eng. Mater.* 2024, 27(2):2401546.
[64] Wu F, Li Y, Wang M. Research on extrusion photocuring-assisted forming process for ceramic 3D printing. *J. Northeast. Univ. (Nat. Sci. Ed.)* 2022, 43(9):1283–1290.
[65] Huang W, Zu Z, Huang Y, Xiang H, Liu X. UV-curing 3D printing of high-performance, recyclable, biobased photosensitive resin enabled by dual-crosslinking networks. *Addit. Manuf.* 2024, 91:104352.
[66] Miao H, Huang Z, Cheng L, Shi W. Syntheses and properties of fluorinated phosphate acrylates used for UV-curing coatings. *Prog. Org. Coat.* 2008, 64(4):365–370.
[67] Zhou Q, Lin J, Li Q. Study of high-strength, low-shrinkage dental resin composites with bifunctional polysilsesquioxane. *Dent. Mater.* 2025, 41(6):755–767.
[68] Liu F, Wang Y, Xue X, Yang H. UV curable EA-Si hybrid coatings prepared by combination of radical and cationic photopolymerization. *Prog. Org. Coat.* 2015, 85:46–51.
[69] Liu H, Liu X, Rao Y, Shen X, Tang Z, *et al.* Facile fabrication of robust and universal UV-curable polyurethane composite coatings with antibacterial properties. *Polym. Eng. Sci.* 2023, 63(10):3371–3381.
[70] Li C, Yuan Y, Liu R, Liu X. Research progress on photocuring reactions with low shrinkage. *Paint Coat. Ind.* 2017, 47(6):81–87.
[71] Wen M, Scriven L, McCormick A. Differential scanning calorimetry and cantilever deflection studies of polymerization kinetics and stress in ultraviolet curing of multifunctional (meth)acrylate coatings. *Macromolecules* 2002, 35(1):112–120.
[72] Yu H, Mhaisalkar S, Wong E. Direct measurement of cure-induced stress in thermosetting materials by means of a dynamic mechanical analyzer. *Macromol. Rapid Commun.* 2006, 27(16):1393–1397.
[73] Stansbury J, Trujillo-Lemon M, Lu H, Ding X, Lin Y, *et al.* Conversion-dependent shrinkage stress and strain in dental resins and composites. *Dent. Mater.* 2005, 21(1):56–67.
[74] He J, Luo Y, Liu F, Jia D. Synthesis and characterization of a new trimethacrylate monomer with low polymerization shrinkage and its application in dental restoration materials. *J. Biomater. Appl.* 2010, 25(3):235–249.
[75] Amirouche-Korichi A, Mouzali M, Watts D. Effects of monomer ratios and highly radiopaque fillers on degree of conversion and shrinkage-strain of dental resin composites. *Dent. Mater.* 2009, 25(11):1411–1418.
[76] Chen C, Huang C, Lin S, Han J, Hsieh K, *et al.* Low-shrinkage visible light-curable urethane-modified epoxy acrylate/SiO_2 composites as dental restorative materials. *Compos. Sci. Technol.* 2008, 68(13):2811–2817.

[77] Manojlovic D, Dramićanin M, Milosevic M, Zeković I, Cvijović-Alagić I, *et al.* Effects of a low-shrinkage methacrylate monomer and monoacylphosphine oxide photoinitiator on curing efficiency and mechanical properties of experimental resin-based composites. *Mater. Sci. Eng.: C* 2016, 58:487–494.

[78] Khoun L, Hubert P. Cure shrinkage characterization of an epoxy resin system by two in situ measurement methods. *Polym. Compos.* 2010, 31(9):1603–1610.

[79] Billotte C, Bernard F, Ruiz E. Chemical shrinkage and thermomechanical characterization of an epoxy resin during cure by a novel *in situ* measurement method. *Eur. Polym. J.* 2013, 49(11):3548–3560.

[80] Cheng X, Guo L, Fu P. Room-temperature, low-pressure nanoimprinting based on cationic photopolymerization of novel epoxysilicone monomers. *Adv. Mater.* 2005, 17(11):1419–1424.

[81] Ye S, Cramer N, Smith I, Voigt K, Bowman C. Reaction kinetics and reduced shrinkage stress of thiol-yne-methacrylate and thiol-yne-acrylate ternary systems. *Macromolecules* 2011, 44(23):9084–9090.

[82] Geiser V, Leterrier Y, Manson J. Conversion and shrinkage analysis of acrylated hyperbranched polymer nanocomposites. *J. Appl. Polym. Sci.* 2009, 114(4):1954–1963.

[83] Satterthwaite J, Vogel K, Watts D. Effect of resin-composite filler particle size and shape on shrinkage-strain. *Dent. Mater.* 2009, 25(12):1612–1615.

[84] Jiang Y. Preparation of grass-derived nanocellulose composite gelatin and research on forming process of bio-3D printed skin scaffolds. Doctoral Thesis, Yangzhou University, 2018.

[85] Chen J, Qiao H, Zheng B, Zhang H. Progress in interfacial rheology of multiphase polymeric systems (In Chinese). *Polym. Bull.* 2025, 38(8):1218–1248.

[86] Ding Z, Zhang C, Li C, Zhang Y, Liu Y, *et al.* Ultraviolet-assisted material extrusion of silicones with largely enhanced mechanical properties and isotropy. *Addit. Manuf.* 2024, 80:103965.

[87] Gómez-Blanco J, Pagador J, Galván-Chacón V, Sánchez-Peralta L, Matamoros M, *et al.* Computational simulation-based comparative analysis of standard 3D printing and conical nozzles for pneumatic and piston-driven bioprinting. *Int. J. Bioprint.* 2023, 9(4):730–730.

[88] Ding Z. Research on UV-assisted direct-write 3d printing technology for silicone elastomers. Master's Thesis, Jiangnan University, 2024.

[89] Gao X, Kim H, Hwang W. Flow modeling in a metering section of a single screw extruder with a small helix angle based on the energy dissipation rate. *Int. J. Multiphase Flow* 2024, 65(3):1081–1092.

[90] Chowdhury M, Islam M, Hossain M, Molla M. Magnetohydrodynamics mixed convection and sensitivity analysis of non-Newtonian power-law fluid in a ventilated cavity with a rotating heated cylinder. *J. Taibah Univ. Sci.* 2024, 18(1):2427386.

[91] Liang J. Study on wall slip behavior of nr/cbr compounds during extrusion-part I: pressure oscillation phenomenon. *Elastomers* 1992, 2(4):37–41.

[92] Griffith M, Halloran J. Scattering of ultraviolet radiation in turbid suspensions. *Appl. Phys.* 1997, 81(6):2538–2546.

[93] Wu K, Seefeldt K, Solomon M, Halloran J. Prediction of ceramic stereolithography resin sensitivity from theory and measurement of diffusive photon transport. *J. Appl. Phys.* 2005, 98(2):024902.

[94] Chartier T, Badev A, Abouliatim Y, Lebaudy P, Lecamp L. Stereolithography process: influence of the rheology of silica suspensions and of the medium on polymerization kinetics-cured depth and width. *J. Eur. Ceram. Soc.* 2012, 32(8):1625–1634.

[95] Hodaei A, Akhlaghi O, Khani N, Aytas T, Sezer D, *et al*. Single additive enables 3D printing of highly loaded iron oxide suspensions. *ACS Appl. Mater. Interfaces* 2018, 10(11):9873–9881.

[96] Pei K, Li S, Cao B, Wang M, Liu M. Catalytic thermocuring and synergistic photothermocuring of single-component acrylate- grafted liquid oligosilazanes. *ACS Omega* 2024, 9(23):24959–24969.

[97] Bouschlicher M, Rueggeberg F, Boyer D. Effect of stepped light intensity on polymerization force and conversion in a photoactivated composite. *J. Esthet. Dent.* 2000, 12(1):23–32.

[98] Dufaud O, Corbel S. Oxygen diffusion in ceramic suspensions for stereolithography. *Chem. Eng. J.* 2003, 92(1–3):55–62.

[99] Ramos-Dez S, Diaz-Gomez L, Paulis M, Camarero-Espinosa S. Multilayer dual-porosity 3D printed scaffolds to recreate the anisotropic microenvironment of the hyaline cartilage. *Mater. Today Bio*. 2025, 102280.